



Article

Hybrid entanglement carrying orbital angular momentum

Fengyi Xu^{a,1}, Meihong Wang^{a,b,1}, Chenyu Qiao^a, Shujing Li^{a,b,*}, Hai Wang^{a,b}, Xiaolong Su^{a,b,*}^aState Key Laboratory of Quantum Optics Technologies and Devices, Institute of Opto-Electronics, Shanxi University, Taiyuan 030006, China^bCollaborative Innovation Center of Extreme Optics, Shanxi University, Taiyuan 030006, China

ARTICLE INFO

Article history:

Received 8 August 2024

Received in revised form 7 November 2024

Accepted 24 December 2024

Available online 7 January 2025

Keywords:

Entanglement

Cat state

Orbital angular momentum

Hybrid entanglement

ABSTRACT

Hybrid continuous-variable (CV) and discrete-variable (DV) entanglement is an essential quantum resource of hybrid quantum information processing, which enables one to overcome the intrinsic limitations of CV and DV quantum protocols. Besides CV and DV quantum variables, introducing more degrees of freedom provides a feasible approach to increase the information carried by the entangled state. Among all the degrees of freedom of photons, orbital angular momentum (OAM) has potential applications in enhancing the communication capacity of quantum communication and precision of quantum measurement. Here, we present the experimental preparation of hybrid entanglement carrying OAM, which involves three degrees of freedom including polarization, cat states, and OAM. By converting the wavefront of optical cat states with a q-plate, the OAM degree of freedom is introduced into the prepared hybrid entanglement between a polarization-encoded DV qubit and a cat-encoded CV qubit. Based on the measured topological charges $l = 0, +1, +2$ and reconstructed Wigner functions of the output states, the hybrid entangled states carrying OAM with $l = 0, +1, +2$ are confirmed with non-zero logarithmic negativities, respectively. Our work takes a crucial step towards extending the degree of freedom for hybrid entanglement, which provides a new quantum resource for hybrid quantum information processing.

© 2025 Science China Press. Published by Elsevier B.V. and Science China Press. All rights are reserved, including those for text and data mining, AI training, and similar technologies.

1. Introduction

After decades of development, tremendous advances have been achieved in both continuous-variable (CV) and discrete-variable (DV) quantum information science and technology [1–7]. In the CV quantum information processing, the quantum variable in the infinite-dimensional Hilbert space, which has a continuum of eigenvalues, is applied to encode information. In the DV quantum information processing, the quantum variable in the finite-dimensional Hilbert space, which is discrete in nature, is involved. The advantage of the CV optical quantum information processing is that the CV optical entangled state is prepared deterministically, but the entanglement degree is limited by the squeezing level [1,2]. The fidelity of CV quantum information processing decreases with the increase of loss since CV entangled state has a limited entanglement degree and is sensitive to loss. On the contrary, the advantage of the DV optical quantum information processing is that the maximum entanglement can be achieved, while the preparation of the DV optical entangled state is probabilistic [8,9]. The successful preparation probability of multi-photon

entanglement decreases with the increase of the number of entangled photons.

To overcome their own intrinsic limitations of CV and DV systems, hybrid CV-DV quantum information processing is developed [10–18], which combines the resources and techniques of both CV and DV systems. For example, the deterministic teleportation of photon qubits (DV state) is demonstrated using CV entanglement as resource [17], and the fidelity in the teleportation of CV state can be increased to 1 using DV entanglement as resource [18]. Especially, hybrid entanglement, which is an essential quantum resource in hybrid quantum information processing, has been experimentally demonstrated, such as that between a single photon and coherent state ($|0\rangle|\alpha\rangle + |1\rangle|-\alpha\rangle$), single photon and cat state ($|0\rangle|\text{cat}_-\rangle + e^{i\varphi}|1\rangle|\text{cat}_+\rangle$), and photon polarization and cat state ($\alpha|H\rangle|\text{cat}_-\rangle + \beta|V\rangle|\text{cat}_+\rangle$) [19–21]. In these demonstrated hybrid entanglement, the entanglement between a polarization-encoded DV qubit and a cat-encoded CV qubit is more suitable for quantum communication, because the polarization qubit is insensitive to loss and beneficial to long-distance transmission [21–24]. For example, the DV qubit of the hybrid CV-DV entanglement can be used to mitigate the decrease of fidelity in the transmission since it is insensitive to loss [22]. Recently, it has been shown that the hybrid CV-DV entanglement can be used to construct a heterogeneous quantum network [25].

* Corresponding authors.

E-mail addresses: lishujing@sxu.edu.cn (S. Li), suxl@sxu.edu.cn (X. Su).¹ These authors contributed equally to this work.

Towards the application of entanglement, it is essential to extend the degrees of freedom of the entangled state, which enables the entangled state to carry more information. Among all the degrees of freedom of photons, the orbital angular momentum (OAM) has attracted much more attention, since it has potential applications in quantum communication [26–29] and quantum precision measurement [30–32]. The OAM beam has a spatial phase form of $\exp[iil\varphi]$ ($l = 0, \pm 1, \pm 2, \dots$), where l is the topological charge number and φ is the azimuthal angle [33,34]. OAM beams with different l can be used to define a high-dimension Hilbert space because they are intrinsically orthogonal and can be efficiently separated. For instance, terabit free-space data transmission has been achieved by employing OAM multiplexing [35], and the two-photon entanglement with high-dimensional OAM have been prepared [36–40]. Besides the DV quantum states carrying OAM, the OAM has also been introduced into the CV quantum states, such as CV multipartite entanglement [41,42], quantum steering [43,44], and hyperentanglement [45,46]. Furthermore, the quantum memory for various quantum states carrying OAM has been demonstrated in an atomic ensemble or a solid-state system [47–49].

Besides the CV and DV quantum states carrying OAM degree of freedom demonstrated in the previous experiments, it has also been shown that a hybrid polarization-OAM entangled state can be obtained by entangling the polarization and OAM of photons [50–52]. Compared to the hybrid polarization-OAM entangled state, it is more important to introduce OAM to the hybrid CV-DV entanglement, since more degrees of freedom are involved in this case. Although quantum state carrying OAM and hybrid CV-DV entanglement have been demonstrated individually, how to prepare the hybrid CV-DV entanglement carrying OAM is still unclear.

Here, we experimentally prepare the hybrid CV-DV entanglement carrying OAM which is a hybrid quantum state involving three kinds of degrees of freedom. We propose a scheme to introduce the OAM degree of freedom to the hybrid CV-DV entanglement by changing the wavefronts of the CV and/or DV photons. Then, we experimentally prepare the hybrid polarization-cat entangled state firstly, and then introduce the OAM degree of freedom by inserting a q-plate in the cat-encoded CV part, which converts the Gaussian beam to the OAM beam. In the characterization of the prepared hybrid state, we measure the OAM property in the CV part, and the entanglement between the polarization-encoded DV part and cat-encoded CV part carrying OAM, respectively. Based on the reconstructed two-mode density matrix in the bases of polarization and cat state, we quantify the entanglement of the hybrid states carrying OAM with $l = 0, +1, +2$ by the logarithmic negativities, which are 0.56 ± 0.01 , 0.52 ± 0.01 , and 0.55 ± 0.01 , respectively. The presented results demonstrate a hybrid state involving polarization, cat state, and OAM degrees of freedom, which has potential applications in quantum communication between heterogeneous quantum nodes.

2. The principle

Fig. 1 presents the scheme of introducing OAM to the hybrid CV-DV entangled state. Here we take the hybrid entangled state between a polarization-encoded DV qubit and a cat-encoded CV qubit $\alpha|H\rangle|\text{cat}_-\rangle + e^{i\theta}\beta|V\rangle|\text{cat}_+\rangle$ as an example, where $|H\rangle$ and $|V\rangle$ represent the polarizations of a single photon, α and β are the probability amplitudes [53–56],

$$\begin{aligned} |\text{cat}_+\rangle &= (|i\alpha_+\rangle + |-i\alpha_+\rangle)/\sqrt{2(1 + e^{-2|\alpha_+|^2})}, \\ |\text{cat}_-\rangle &= (|i\alpha_-\rangle - |-i\alpha_-\rangle)/\sqrt{2(1 - e^{-2|\alpha_-|^2})}, \end{aligned} \quad (1)$$

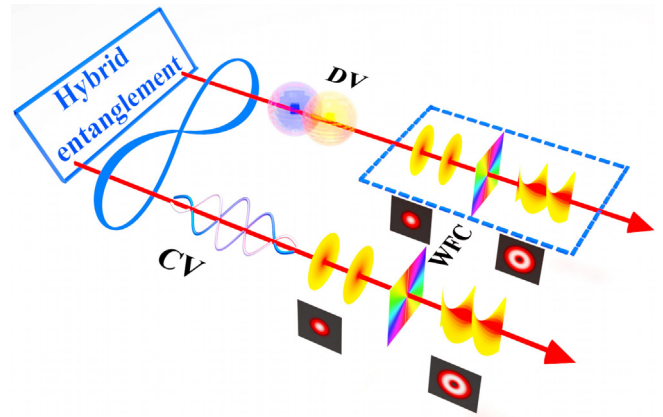


Fig. 1. The schematic of hybrid CV-DV entanglement carrying OAM. The wavefront of photons (DV part) and cat state (CV part) of the hybrid entangled state is converted from Gaussian distribution to OAM mode by the wavefront converter (WFC). The WFC in the dashed box is removed in the preparation of the hybrid entangled state carrying OAM in the CV part.

are the even and odd cat states respectively, and θ is the phase difference between two terms in the entangled state.

To prepare the hybrid entangled state carrying OAM, a wavefront converter, which is composed of two quarter-wave plates and a q-plate, is inserted in the path of the CV and/or DV parts to transform the Gaussian beams with planar wavefront into an OAM mode. After introducing the OAM to this state, the obtained hybrid entangled state carrying OAM is given by

$$|\psi\rangle = \alpha|H\rangle_{l_b}|\text{cat}_-\rangle_{l_c} + e^{i\theta}\beta|V\rangle_{-l_b}|\text{cat}_+\rangle_{l_c}, \quad (2)$$

where the subscript l_b (l_c) denotes the topological charge of the OAM mode carried by the horizontal polarization photons in the DV part (cat states in the CV part). In this case, the topological charge of the OAM mode carried by the vertical polarization photons in the DV part should be $-l_b$, because a q-plate introduces opposite topological charges of the OAM mode for left- and right-circularly polarized lights. It is obvious that various hybrid states carrying OAM mode can be prepared when different l_b and l_c are applied.

In our experiment, the photon in the DV part is directed to a single photon detector through a single-mode fiber. Since the OAM carried by the photon in the DV part is transformed to Gaussian mode after the single-mode fiber, i.e., the helical wavefront is erased, we only introduce the OAM to the CV part of the hybrid entangled state. The obtained hybrid entangled state is given by

$$|\psi\rangle_l = \alpha|H\rangle|\text{cat}_-\rangle_l + e^{i\theta}\beta|V\rangle|\text{cat}_+\rangle_l. \quad (3)$$

3. Experimental setup

Fig. 2 shows the experimental setup. A 795 nm continuous Ti-sapphire laser, which corresponds to the storage band of rubidium atoms, is used as the laser source. A part of the laser beam is injected into a bow-tie ring cavity containing a periodically poled KTiOPO₄ (PPKTP) crystal for second harmonic generation (SHG) [53]. The output beam at 397.5 nm is used as the pump beam of the optical parametric amplifier (OPA), which is employed to generate the squeezed vacuum state. By locking the relative phase difference between the pump beam and the seed beam of the OPA to π , an amplitude-squeezed state with squeezing of -1.9 dB for the bandwidth of 13 MHz is prepared.

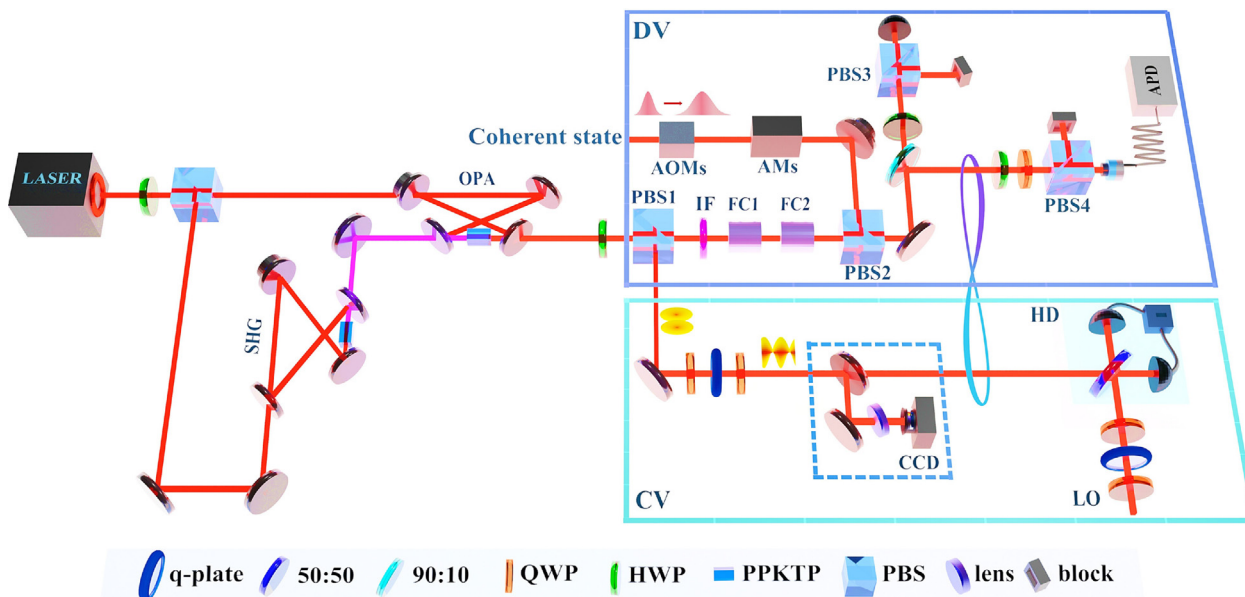


Fig. 2. The experimental setup for preparing hybrid polarization-cat entanglement carrying OAM. An odd or even cat state is prepared in the CV part when a photon is subtracted from the squeezed vacuum state by a HWP and PBS1 or not. The wavefront of the superposition of the even and odd cat states is transformed to OAM mode after passing a q-plate and two QWPs. The subtracted photon and an attenuated coherent state are coupled on PBS2 and detected by an APD. The interference signal between the output beam of OPA and the weak coherent beam is detected from the transmission port of PBS3 and is used for phase locking. Conditioned on the click of the APD the hybrid polarization-cat entanglement carrying OAM is prepared. SHG: second harmonic generator, OPA: optical parametric amplifier, PPKTP: periodically poled KTiOPO₄, PBS: polarization beam-splitter, IF: interference filter, FC: filter cavity, AOM: acousto-optic modulator, AM: amplitude modulator, HWP: half-wave plate, QWP: quarter-wave plate, CCD: charge-coupled device, HD: homodyne detector, LO: local oscillator, APD: avalanche photodiode.

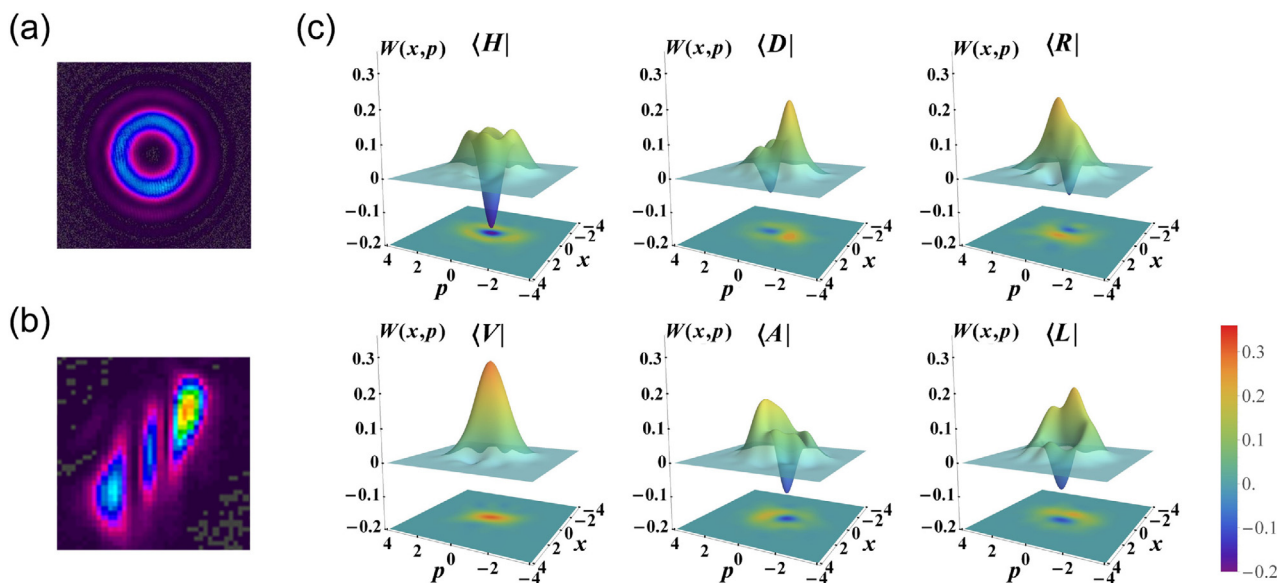


Fig. 3. The results of the prepared hybrid state carrying OAM with $l = +2$. (a) The measured spatial profile and (b) the interference-like patterns of the CV part of the hybrid state. (c) The Wigner functions and corresponding contours of the CV part of the hybrid state, when projecting the DV part on different polarization bases. All results are corrected for a detection efficiency of 80%. The fidelities of the reduced hybrid states are 0.76, 0.94, 0.69, 0.66, 0.73 and 0.74 for the projection bases $\langle H|$, $\langle V|$, $\langle D|$, $\langle A|$, $\langle R|$ and $\langle L|$, respectively. The negativities of Wigner functions of the reduced hybrid states are -0.19 , -0.07 , -0.11 , -0.10 and -0.08 for the projection bases $\langle H|$, $\langle D|$, $\langle A|$, $\langle R|$ and $\langle L|$, respectively.

The generated squeezed vacuum state is used to approximate the even cat state $|\text{cat}_+\rangle$ with amplitude of $\alpha_+ = 0.5$ since the fidelity between the even cat state and the prepared squeezed vacuum state is about 0.97. By subtracting a photon from the squeezed vacuum state, which is implemented by a combination of a half-wave plate (HWP) and a polarization beam-splitter (PBS1) with a transmittance of 4.5%, an odd cat state $|\text{cat}_-\rangle$ with amplitude of $\alpha_- = 0.86$ is obtained (see the Supplementary material for more details).

The reflected optical beam from the PBS1 serves as the CV part of the hybrid entanglement, which is a superposition of the even and odd cat states. The subtracted photon with horizontal polarization and a photon from the attenuated weak coherent beam with vertical polarization are coupled on the PBS2 and the output of it serves as the DV part of the hybrid entanglement.

In the preparation of the hybrid CV-DV entanglement, the most technical challenge comes from the mismatch of the bandwidth

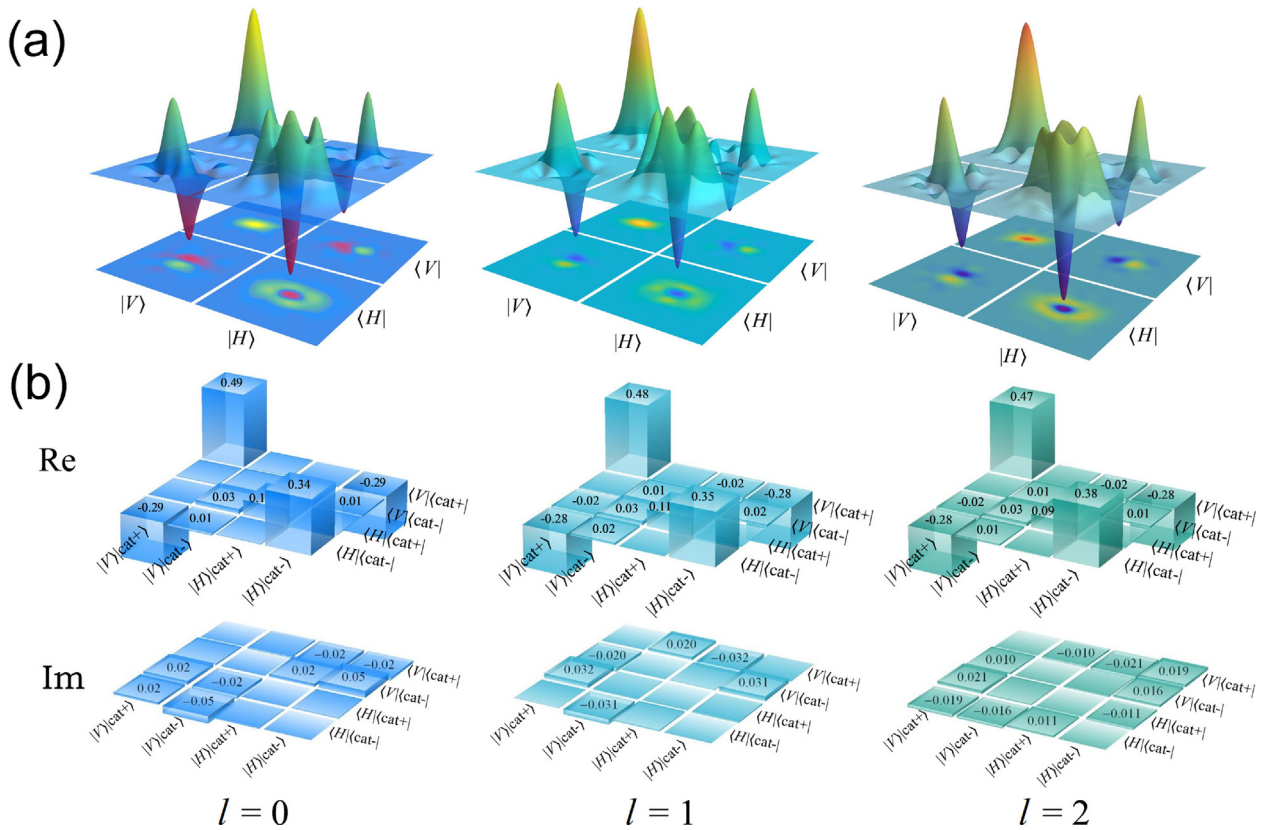


Fig. 4. The results of the hybrid entanglement carrying OAM with $l = 0, +1, +2$. (a) Wigner functions associated with the reduced density matrices $\langle m|\hat{\rho}|n\rangle$ with $m, n \in \{H, V\}$. (b) Reconstructed density matrices for prepared hybrid entangled states in the basis of $\{|H\rangle, |V\rangle\} \otimes \{|cat\rangle_+, |cat\rangle_-\}$. The real and imaginary parts are shown in top and bottom rows, respectively.

between the subtracted photon and the approximated single photon in the DV part, which are 13 and 2.5 MHz, respectively. To solve this problem and ensure these photons are indistinguishable, we extend the bandwidth of the weak coherent beam by using two acousto-optic modulators (AOMs). After passing the AOMs, the coherent state is shaped into a pulse with the bandwidth of about 12 MHz by applying a square wave with the duration of 134 ns. To obtain an approximated single photon, these two AOMs with diffractive efficiency of 10% and three amplitude modulators (AMs) are applied to attenuate a $5 \mu\text{W}$ coherent beam for 90 dB (see the Supplementary material for more details). In this case, the attenuated coherent state spectrum is shaped to optimal overlap with the subtracted photon spectrum, so that the spectral part of the single photon quantum state factors out from the polarization part. When a photon in the DV part is detected, it means that the generation of the hybrid CV-DV entanglement.

To introduce the OAM degree of freedom to the hybrid CV-DV entanglement, a wavefront converter with the transmittance of 98% that consists of two quarter-wave plates (QWPs) and a q-plate (VR-780, lbttek) is inserted in the path of the CV part. After the first QWP, the Gaussian beam with vertical polarization in the CV part is changed to left-circular polarization, which is the requirement of the q-plate. The wavefront of the Gaussian beam is transformed to OAM mode after the q-plate, and then the polarization of the OAM mode is changed from circular polarization to vertical polarization after the second QWP. In order to measure the CV part carrying OAM with a homodyne detector, a wavefront converter is also inserted in the path of the local oscillator (LO) to make sure the OAM with the opposite topological charge is carried by the LO. After the 50:50 beam-splitter (BS), the topological charge $-l$ of OAM carried by the reflected beam is changed to l ,

which is the same as that of the transmitted beam. In this case, the efficient interference between the CV part of the hybrid state and the LO is guaranteed in the homodyne detection. The interference efficiency between the CV part and the LO decreases with the increase of the topological charge of OAM mode, which leads to the decrease of the fidelity of the measured hybrid entangled state. The interference efficiencies exceed 97% for OAM with $l = 0, +1, +2$ are obtained in our experiment.

In order to characterize the prepared hybrid state carrying OAM, we measure both topological charge of OAM and entanglement of the hybrid state. In the verification of topological charge of OAM, we measure both spatial profile and interference-like patterns of the prepared hybrid state carrying OAM with a charge-coupled device (CCD) camera and a tilted lens, as shown in the dashed box in Fig. 2. After the twice reflection, the output beam of the wavefront converter enters into a CCD camera to record spatial distribution. To identify the topological charge of OAM, we insert a tilted lens with $R = 70$ mm in front of the CCD camera, where a transverse intensity profile with symmetric interference-like patterns is presented [57].

To characterize the entanglement of the hybrid state, we project the DV part of the state to six polarization bases $|H\rangle, |V\rangle, |D\rangle = (|H\rangle + |V\rangle)/\sqrt{2}, |A\rangle = (|H\rangle - |V\rangle)/\sqrt{2}, |R\rangle = (|H\rangle + i|V\rangle)/\sqrt{2}, |L\rangle = (|H\rangle - i|V\rangle)/\sqrt{2}$ by a polarization projection system, and implement the quantum tomography on the CV part to reconstruct the corresponding Wigner functions, respectively. The output photon from the polarization projection system, which consists of a HWP, a QWP, and PBS4, is coupled into an avalanche photodiode (APD) through a single-mode fiber. To obtain a hybrid entangled state with maximum entanglement, the intensity of the weak beam is adjusted to warrant equal probability for having $|H\rangle$

or $|V\rangle$ after PBS2. In this case, the probability amplitude $\alpha = \beta = 1/\sqrt{2}$ in Eq. (3) is obtained for the prepared hybrid entangled state.

4. Results

The measured spatial profile and interference-like patterns of the hybrid state carrying OAM with $l = +2$, are shown in Fig. 3a and b respectively, which confirms the OAM mode is generated after the wavefront converter. In the measured symmetric interference-like patterns of the intensity distribution, the orientation of the stripes ($+45^\circ$) and the number of the bright stripes n ($n = 3$) indicate the sign and magnitude ($|l| = n - 1$) of the topological charge of OAM, respectively. As shown in Fig. 3b, it is obvious that the topological charge $l = +2$ of OAM is carried by the CV part of the hybrid state.

When the topological charge of OAM is set to $l = 0, +1, +2$, we reconstruct the corresponding Wigner functions of the CV part of the hybrid state by projecting the DV part on six polarization bases, respectively. Using the maximum-likelihood algorithm [58], the Wigner functions are obtained from the reconstructed density matrices in Fock basis, which are presented in Figs. S2–S4 (online). The reconstructed Wigner functions for the reduced hybrid state carrying OAM with $l = +2$ are shown in Fig. 3c. When the DV part is projected on $|H\rangle$ and $|V\rangle$ bases, the CV part is collapsed to a photon-subtracted squeezed vacuum state (an approximate odd cat state) with negativity of $W(0,0) = -0.19$ and a squeezed vacuum state (an approximate even cat state), respectively. When the DV part is projected on a superposition of $|H\rangle$ and $|V\rangle$ bases, the CV part is collapsed to a corresponding superposition of the squeezed vacuum state and the photon-subtracted squeezed vacuum state. Specifically, projecting the DV part onto $|D\rangle$ and $|A\rangle$ bases, the Wigner functions of the CV part exhibit two approximate Gaussian peaks with opposite displacement along phase-quadrature in phase space. Projecting the DV part onto $|R\rangle$ and $|L\rangle$ bases, the positive peaks of the Wigner functions are observed along amplitude-quadrature respectively, which is consistent with the theoretical prediction. The detailed experimental results of the hybrid state carrying OAM with $l = 0, +1$ can be found in Figs. S5 and S6 (online).

In order to visually characterize the prepared two-mode entanglement between polarization-encoded DV qubit and the cat-encoded CV qubit, we show the Wigner functions associated with the reduced density matrices $\hat{\rho}_{mn} = \langle m|\hat{\rho}|n\rangle$ in a matrix form for the hybrid state carrying OAM with $l = 0, +1, +2$ in Fig. 4a, where m (n) denotes the polarization basis $|H\rangle$ or $|V\rangle$. In this case, the diagonal elements in Fig. 4a represent the Wigner functions of the squeezed vacuum state and the photon-subtracted squeezed state, respectively, which are reconstructed from the measured $\hat{\rho}_{HH}$ and $\hat{\rho}_{VV}$ in Fig. 3c in the bases of $|H\rangle$ and $|V\rangle$. The off-diagonal terms are the Wigner functions corresponding to $\hat{\rho}_{HV}$ and $\hat{\rho}_{VH}$, which are obtained from the measured reduced density matrices $\hat{\rho}_{DD}, \hat{\rho}_{AA}, \hat{\rho}_{RR}$ and $\hat{\rho}_{LL}$ in Fig. 3c according to $\hat{\rho}_{HV} = \hat{\rho}_{VH}^\dagger = \frac{1}{2}(\hat{\rho}_{DD} - \hat{\rho}_{AA} + i\hat{\rho}_{LL} - i\hat{\rho}_{RR})$. The non-zero off-diagonal terms represent the coherence of superposition of $|\text{cat}_-\rangle_l$ and $|\text{cat}_+\rangle_l$ in the hybrid state.

Then we calculate the fidelity of the prepared state in the bases of polarization and cat states $\{|H\rangle, |V\rangle\} \otimes \{|\text{cat}_+\rangle_l, |\text{cat}_-\rangle_l\}$ to verify the similarity between the prepared state and the theoretical predicted hybrid state. The density matrices in the cat-state basis $\{|\text{cat}_+\rangle_l, |\text{cat}_-\rangle_l\}$ are obtained by transforming the diagonal elements ($\hat{\rho}_{HH}$ and $\hat{\rho}_{VV}$) and the off-diagonal terms ($\hat{\rho}_{HV}$ and $\hat{\rho}_{VH}$) presented in Fig. 4a into the cat-state basis (see the Supplementary material for more details). The reconstructed density matrices of the hybrid states carrying OAM with $l = 0, +1, +2$, in the basis $\{|H\rangle, |V\rangle\} \otimes \{|\text{cat}_+\rangle_l, |\text{cat}_-\rangle_l\}$ are shown in Fig. 4b. The fidelity of

the hybrid state with ideal state $|\psi_{\text{ideal}}\rangle$ is evaluated by $F = \langle \psi_{\text{ideal}}|\hat{\rho}|\psi_{\text{ideal}}\rangle$, where the ideal state is $|\psi_{\text{ideal}}\rangle = (|H\rangle|\text{cat}_-\rangle_l - |V\rangle|\text{cat}_+\rangle_l)/\sqrt{2}$ (see the Supplementary material for more details). For the prepared hybrid states carrying OAM with $l = 0, +1, +2$, the fidelities of them are 0.71 ± 0.01 , 0.69 ± 0.01 , and 0.70 ± 0.01 , respectively. All fidelities exceed the classical limit of 0.5, which indicates the existence of entanglement in the prepared hybrid states carrying OAM.

Furthermore, to quantify the entanglement of the hybrid state, we calculate the logarithmic negativity of the prepared hybrid state carrying OAM by $E_N(\hat{\rho}) = \log_2 \|\hat{\rho}^{TA}\|_1$, where $\hat{\rho}^{TA}$ is the partial transpose of $\hat{\rho}$ with respect to DV part [59]. The trace norm of $\hat{\rho}^{TA}$ is $\|\hat{\rho}^{TA}\|_1 = 2N(\hat{\rho}) + 1$, where $N(\hat{\rho})$ is the absolute value of the sum of negative eigenvalues of $\hat{\rho}^{TA}$. By transposing density matrices shown in Fig. 4b, we obtain the logarithmic negativities of the prepared hybrid states carrying OAM with $l = 0, +1, +2$, which are 0.56 ± 0.01 , 0.52 ± 0.01 , and 0.55 ± 0.01 , respectively. The non-zero logarithmic negativities confirm the successful preparation of the hybrid entanglement carrying OAM in our experiment.

5. Discussion and conclusion

By introducing the OAM degree of freedom to the CV part of the hybrid entangled state, more information can be carried compared to the traditional hybrid CV-DV entanglement. Besides introducing the OAM degree of freedom to the CV part of the hybrid entanglement, it can also be introduced to the DV part of the hybrid entanglement. In this case, various hybrid entangled states carrying OAM can be prepared as predicted in Eq. (2), where much more information can be encoded with such states. To measure the photons carrying OAM in the DV part, the single photon detection system has to be updated to match the OAM modes. More interestingly, a hyperentangled state in three degrees of freedom can be prepared by introducing OAM into the hybrid CV-DV entanglement, which is a challenging project and worthwhile for further investigation.

In summary, we propose a scheme to introduce the degree of freedom OAM to a hybrid CV-DV entangled state and experimentally demonstrate the hybrid entanglement carrying OAM with topological charges of $l = 0, +1, +2$. The OAM property in the CV part of the hybrid state is verified by measuring the spatial profile and interference-like pattern. The entanglement of the hybrid entangled state carrying OAM is quantified by logarithmic negativity, which is obtained from the density matrices in the bases of polarization and cat states. We show that logarithmic negativities of 0.56 ± 0.01 , 0.52 ± 0.01 , and 0.55 ± 0.01 are obtained for the hybrid entangled states carrying OAM with $l = 0, +1, +2$, respectively, which confirm the successful preparation of the hybrid entanglement carrying OAM in our experiment. The prepared hybrid entanglement has potential applications in increasing the information capacity of quantum communication in the heterogeneous quantum network [25]. Our work demonstrates the feasibility of introducing OAM degree of freedom into the hybrid entanglement and takes a crucial step towards hybrid quantum information processing with multiple degrees of freedom.

Conflict of interest

The authors declare that they have no conflict of interest.

Acknowledgments

This work was financially supported by the National Natural Science Foundation of China (12434015, 11834010, and 62275145), the Fundamental Research Program of Shanxi Province

(20210302121002), and the Fund for Shanxi "1331 Project" Key Subjects Construction.

Author contributions

Xiaolong Su, Shujing Li, and Hai Wang designed the research; Fengyi Xu and Chenyu Qiao performed the research; Fengyi Xu and Meihong Wang contributed new analytic tools; Fengyi Xu, Chenyu Qiao, Meihong Wang and Shujing Li analyzed the data; Fengyi Xu, Shujing Li, Meihong Wang and Xiaolong Su wrote the paper.

Appendix A. Supplementary material

Supplementary data to this article can be found online at <https://doi.org/10.1016/j.scib.2025.01.003>.

References

- Weedbrook C, Pirandola S, García-Patrón R, et al. Gaussian quantum information. *Rev Mod Phys* 2012;84:621–69.
- Braunstein SL, van Loock P. Quantum information with continuous variables. *Rev Mod Phys* 2005;77:513–77.
- Horodecki R, Horodecki P, Horodecki M, et al. Quantum entanglement. *Rev Mod Phys* 2009;81:865–942.
- Su X, Wang M, Yan Z, et al. Quantum network based on non-classical light. *Sci China Inf Sci* 2020;63:180503.
- Sangouard N, Simon C, de Riedmatten H, et al. Quantum repeaters based on atomic ensembles and linear optics. *Rev Mod Phys* 2021;83:33–80.
- Simon C. Towards a global quantum network. *Nat Photonics* 2017;11:678–80.
- Wehner S, Elkouss D, Hanson R. Quantum internet: a vision for the road ahead. *Science* 2018;362:eaam9288.
- Duan L-M, Lukin MD, Cirac JI, et al. Long-distance quantum communication with atomic ensembles and linear optics. *Nature* 2001;414:413–8.
- van Leent T, Bock M, Garthoff R, et al. Long-distance distribution of atom-photon entanglement at telecom wavelength. *Phys Rev Lett* 2020;124:010510.
- Andersen UL, Neergaard-Nielsen JS, van Loock P, et al. Hybrid discrete and continuous variable quantum information. *Nat Phys* 2015;11:713–9.
- van Loock P. Optical hybrid approaches to quantum information. *Laser Photon Rev* 2011;5:167–200.
- van Loock P, Munro WJ, Nemoto K, et al. Hybrid quantum computation in quantum optics. *Phys Rev A* 2008;78:022303.
- Ren S, Wang Y, Su X. Hybrid quantum key distribution network. *Sci China Inf Sci* 2022;65:200502.
- Ulanov AE, Sychev D, Pushkina AA, et al. Quantum teleportation between discrete and continuous encodings of an optical qubit. *Phys Rev Lett* 2017;118:160501.
- Lee N, Benichi H, Takeno Y, et al. Teleportation of nonclassical wave packets of light. *Science* 2011;332:330–3.
- Takeda S, Fuwa M, van Loock P, et al. Entanglement swapping between discrete and continuous variables. *Phys Rev Lett* 2015;114:100501.
- Takeda S, Mizuta T, Fuwa M, et al. Deterministic quantum teleportation of photonic quantum bits by a hybrid technique. *Nature* 2013;500:315–8.
- Andersen UL, Ralph TC. High-fidelity teleportation of continuous-variable quantum states using delocalized single photons. *Phys Rev Lett* 2013;111:050504.
- Jeong H, Zavatta A, Kang M, et al. Generation of hybrid entanglement of light. *Nat Photonics* 2014;8:564–9.
- Morin O, Huang K, Liu J, et al. Remote creation of hybrid entanglement between particle-like and wave-like optical qubits. *Nat Photonics* 2014;8:570–4.
- Sychev DV, Ulanov AE, Tiunov ES, et al. Entanglement and teleportation between polarization and wave-like encodings of an optical qubit. *Nat Commun* 2018;9:3672.
- Kwon H, Jeong H. Generation of hybrid entanglement between a single-photon polarization qubit and a coherent state. *Phys Rev A* 2015;91:012340.
- Sheng Y-B, Zhou L, Long G-L. Hybrid entanglement purification for quantum repeaters. *Phys Rev A* 2013;88:022302.
- Li S, Yan H, He Y, et al. Experimentally feasible generation protocol for polarized hybrid entanglement. *Phys Rev A* 2018;98:022334.
- Guccione G, Darras T, Jeannic HL, et al. Connecting heterogeneous quantum networks by hybrid entanglement swapping. *Sci Adv* 2021;6:eaba4508.
- Yao AM, Padgett MJ. Orbital angular momentum: origins, behavior and applications. *Adv Opt Photon* 2011;3:161–204.
- Wang J, Liu J, Li S, et al. Orbital angular momentum and beyond in free-space optical communications. *Nanophotonics* 2017;11:645–80.
- Chen R, Zhou H, Moretti M, et al. Orbital angular momentum waves: generation, detection and emerging applications. *IEEE Commun Surv Tutor* 2020;22:840–68.
- Khouri AZ, Milman P. Quantum teleportation in the spin-orbit variables of photon pairs. *Phys Rev A* 2011;83:060301.
- Lavery MPJ, Speirits FC, Barnett SM, et al. Detection of a spinning object using light's orbital angular momentum. *Science* 2013;341:537–40.
- D'Ambrosio V, Spagnolo N, Del Re L, et al. Photonic polarization gears for ultra-sensitive angular measurements. *Nat Commun* 2013;4:2432.
- Liu K, Cai C, Li J, et al. Squeezing-enhanced rotating-angle measurement beyond the quantum limit. *Appl Phys Lett* 2018;113:261103.
- Allen L, Beijersbergen MW, Spreeuw RJC, et al. Orbital angular momentum of light and the transformation of Laguerre-Gaussian laser modes. *Phys Rev A* 2019;45:8185–9.
- Agha I. Integrated optical vortex beams: ultrafast orbital angular momentum sources beyond traditional spatial light modulators. *Sci Bull* 2024;69:2647–9.
- Wang J, Yang JY, Fazal I, et al. Terabit free-space data transmission employing orbital angular momentum multiplexing. *Nat Photonics* 2012;6:488–96.
- Dada AC, Leach J, Buller GS, et al. Experimental high-dimensional two-photon entanglement and violations of generalized Bell inequalities. *Nat Phys* 2011;7:677–80.
- Krenn M, Huber M, Fickler R, et al. Generation and confirmation of a (100×100) -dimensional entangled quantum system. *Proc Natl Acad Sci USA* 2014;111:6243–7.
- Mair A, Vaziri A, Weihs G, et al. Entanglement of the orbital angular momentum states of photons. *Nature* 2001;412:313–6.
- Zeng Q, Wang B, Li P, et al. Experimental high-dimensional Einstein-Podolsky-Rosen steering. *Phys Rev Lett* 2018;120:030401.
- Kong L-J, Sun Y-F, Zhang F-R, et al. High-dimensional entanglement-enabled holography. *Phys Rev Lett* 2023;130:053602.
- Marino AM, Boyer V, Pooser RC, et al. Delocalized correlations in twin light beams with orbital angular momentum. *Phys Rev Lett* 2008;101:093602.
- Li S, Pan X, Ren Y, et al. Deterministic generation of orbital-angular-momentum multiplexed tripartite entanglement. *Phys Rev Lett* 2020;124:083605.
- Zeng L, Ma R, Wen H, et al. Deterministic distribution of orbital angular momentum multiplexed continuous-variable entanglement and quantum steering. *Photon Res* 2022;10:777–85.
- Qu R, Wang Y, Zhang X, et al. Robust method for certifying genuine high-dimensional quantum steering with multimeasurement settings. *Optica* 2022;9:473–8.
- dos Santos BC, Dechoum K, Khouri AZ. Continuous-variable hyperentanglement in a parametric oscillator with orbital angular momentum. *Phys Rev Lett* 2009;103:230503.
- Liu K, Guo J, Cai C-X, et al. Experimental generation of continuous-variable hyperentanglement in an optical parametric oscillator. *Phys Rev Lett* 2014;113:170501.
- Ye Y-H, Zeng L, Dong M-X, et al. Detection of a spinning object using light's orbital angular momentum. *Science* 2013;341:537–40.
- Parigi V, D'Ambrosio V, Arnold C, et al. Storage and retrieval of vector beams of light in a multiple-degree-of-freedom quantum memory. *Nat Commun* 2015;6:7706.
- Zhou Z-Q, Hua Y-L, Liu X, et al. Quantum storage of three-dimensional orbital-angular-momentum entanglement in a crystal. *Phys Rev Lett* 2015;115:070502.
- Nagali E, Sciarrino F. Generation of hybrid polarization-orbital angular momentum entangled states. *Opt Express* 2010;18:18243–8.
- Gabriel C, Aiello A, Zhong W, et al. Entangling different degrees of freedom by quadrature squeezing cylindrically polarized modes. *Phys Rev Lett* 2011;106:060502.
- Jabir MV, Chaitanya NA, Mathew M, et al. Direct transfer of classical non-separable states into hybrid entangled two photon states. *Sci Rep* 2017;7:7331.
- Zhang M, Kang H, Wang M, et al. Quantifying quantum coherence of optical cat states. *Photonics Res* 2021;9:887–92.
- Wang M, Zhang M, Qin Z, et al. Experimental preparation and manipulation of squeezed cat states via an all-optical in-line squeezer. *Laser Photonics Rev* 2022;16:2200336.
- Han D, Sun F, Wang N, et al. Remote preparation of optical cat states based on gaussian entanglement. *Laser Photonics Rev* 2023;17:2300103.
- Sun F, Fang Y, He Q, et al. Generating optical cat states via quantum interference of multi-path free-electron-photons interactions. *Sci Bull* 2023;68:1366–71.
- Vaity P, Banerji J, Singh RP. Measuring the topological charge of an optical vortex by using a tilted convex lens. *Phys Lett A* 2013;377:1154–6.
- Lvovsky AI, Raymer MG. Continuous-variable optical quantum-state tomography. *Rev Mod Phys* 2009;81:299.
- Vidal G, Werner RF. Computable measure of entanglement. *Phys Rev A* 2002;65:032314.